PCCP

Accepted Manuscript

ROYAL SOCIETY OF CHEMISTRY

www.rsc.org/pccp

Uniaxial tension-induced fracture in gold nanowires with the dependence of sizes and atomic vacancies

Fenying Wang,[1,*] Yanfeng Dai,[1] Jianwei Zhao,[2] Qianjin Li[2]

[1] *School of Chemistry, Material Science and Engineering, Nanchang University, Nanchang 330031, P. R. China*

[2] *State Key Laboratory of Analytical Chemistry for Life Science, School of Chemistry and Chemical Engineering, Nanjing University, Nanjing 210008, P. R. China*

Email (Corresponding author): [*], wangfenying@ncu.edu.cn.

Abstract

Atomic vacancy plays an important role in the deformation and fracture process of a metallic nanowire subjected to uniaxial tension. However, it is a great challenge for exploring such evolvements by experimental methods. Here, molecular dynamics simulations were used to study the deformation, fracture mechanism and mechanical character of gold nanowires with different atomic vacancies and sizes. Several valuable results were observed. First, the statistical breaking position distributions showed two fracture styles of gold nanowires. The small-sized gold nanowire exhibited a cluster rupture with disordered crystalline structures, and the breaking position appeared in the middle region. While the gold nanowire with large size exhibited an ordered slippage rupture and was apt to break at its two ends. Second, the breaking position distribution of large-sized gold nanowire was more sensitive to atomic vacancies than that of small-sized gold nanowire. Third, the mechanical strength could be improved by decreasing gold nanowire size. Finally, small-sized gold nanowires behaved uncertain characters owing to the surface atom effects.

1. Introduction

The miniaturization of electronics gives great potential applications of nanoscale devices with mechanical properties that are clearly different from those with large dimensions.[1-3] Metallic nanowires, as the main part of electronic devices, have attracted more attentions for their unique properties, particularly the fracture failure behaviors disturbed by surface atoms.[4] More efforts have been devoted to regulate the fracture failure behaviors and other properties of nanowires by constructing atomic defects and vacancies in metal nanowires.[5,6] It is an obvious challenging task using experimental measures[7-9] to explore the evolvements of the atomic structure of nanowires from crystalline to amorphous structure under surface atomic effects and various conditions including strain rate, temperature, crystalline orientation and atomic vacancy. However, molecular dynamics (MD) simulation,[10,11] which solves Newton's equation of motion by collection of interacting atoms over a number of time steps, is an effective method to study the crystalline deformation and corresponding properties of metal nanowires.

For the investigation of sizes and defects effects on the deformation behaviors of nanowires, Diao *et al.*[12] have studied surface-stress-induced phase transformation in metal nanowires, and the MD results showed that the phase transformation was related with the capabilities of overcoming the energy barriers by surface stress at different sizes. By micro-structure design, a near-ideal strength has been discovered in gold nanowires under special defect.[13] The influence of defect on the formation of one-atom constriction in gold nanowires has been presented by Silva *et al.*.[14] We also

discovered that the tensile deformation mechanism was related with a competition between the tensile action and the constructed atomic vacancies at different strain rates[15] and temperatures.[16,17] For the investigation of influences of atomic vacancies at such a small scale, we focused on the microscopic deformation mechanisms and macroscopic fracture behaviors of single-crystal gold nanowires containing atomic vacancies. From the analysis of fracture behaviors, we observed a most probable breaking position when the copper nanowire was subjected to uniaxial tension.[18] Similar behaviors in experiments were also found in the research of metallic and molecular junction conductance.[19,20] Therefore, we designed different initial equilibrium states in this work to study statistically uniaxial tension-induced fracture and the corresponding deformation mechanism of the gold nanowire under the effects of atomic vacancies and nanowire sizes.

2. Methodology

As shown in Figure 1(a), the gold nanowire was generated as a regular lattice of face centered cubic (FCC) along the [100] crystallographic orientation. For computational geometry of FCC crystals, the close packed (111) surface usually exhibits lower surface energy.[21,22] However, the nanowire with [100] orientation, the most typical model of FCC crystalline structures, was selected to study its fracture under the effect of atomic vacancy. To ensure its stability, we have optimized a lot of conditions, such as enough relaxation, the strain rate of 1.0% ps^{-1}, a statistical analysis and a series of comparisons. All of these may reduce systematic errors to ensure the reliability of MD simulations. Regarding the effect of strain rate, 1.0% ps^{-1}, a high

strain rate for any materials and structures from macroscopic viewpoint, was chosen, because the strain rate could be considered as quasi-static state of the gold nanowire, which could avoid the strain rate effect towards different nanowire sizes as much as possible.[15-17]

In this study, two sizes of gold nanowires were selected, (3a × 3a × 9a) and (9a × 9a × 27a) ("*a*" means lattice constant, 0.408 nm for gold). The size selection was according to the previous work considering the influence of nanowire lengths on their fractures.[23] The mean-square error of the stress was a stable value for nanowires with aspect ratio of about (1:3), which indicated that this might be enough to minimize their constrain posed by rigid boundaries on the top and bottom of nanowires. Before stretching, relaxation in three-dimensional space was applied for the gold nanowire under zero traction (*xy*-plane) and zero stress (*z*-direction).[24] In general, with the relax time increasing, when the recorded average potential energy per atom reached a stable state and the stress was fluctuating slightly around 0.0 GPa, we would confirm that the nanowire achieved the equilibration of the system. Then, 300 initial equilibrium states were set at intervals of the same loop (eg. 10,000 loop with the timestep of 1.6 *fs*), which was in accordance with other simulation conditions. After that, 300 initial states with enough and different relax time were adopted for each simulated condition, which were appropriate to ensure the reliability of MD simulations. For too few samples (less than 200) could not give an accurate statistical results about the breaking position distribution, and too many samples (more than 300) would bring some difficulties in calculating the deformation of nanowires.[25] Table 1 gives the

detailed conditions, and a total samples of 4,800 (2×8×300) were done to study the influence of atomic vacancy on the deformation behaviors of gold nanowires at two different sizes. With a strain rate of 1.0% ps^{-1},[15,26] stretching was applied by uniformly moving two fixed layers of the nanowire in the uniaxial tensile direction (*z*-direction). For the fracture of nanowires, our results showed that the nanowire with size I ($3a \times 3a \times 9a$) exhibited disordered cluster rupture, and with size II ($9a \times 9a \times 27a$) exhibited ordered slippage rupture. After statistical analysis, the most probable breaking position of the perfect nanowire ($3a \times 3a \times 9a$) was in the middle region, and the most probable breaking positions were distributed at the two ends of the perfect nanowire ($9a \times 9a \times 27a$). According to the fracture styles of the perfect nanowires with two different sizes, the position of single-layer atomic vacancies was set in the middle of the two fixed layers (0.0 and 1.0) in order to discover the influence of atomic vacancies on two different breaking distribution styles. As is shown in Fig. 1(b) and 1(c), atomic vacancies in the single-layer crystalline plane were controlled to be in a uniform distribution with the fixed vacancy ratio, which is a ratio between atomic vacancies and all atoms in a single-layer crystalline plane.[16] For example, one atomic vacancy was set in the center of the single-layer crystalline plane with ratios being 4% for the size I and 0.6% for the size II. Based on the vacancy sensitivity, atomic vacancy ratios were set from 4% to 35% for size I and from 0.6% to 30% for size II, respectively. For the different atomic vacancy ratios for size I and size II, one atomic vacancy corresponds to the ratio of 4% for size I and the ratio of 0.6% for size II. For the last ratio, it was set according to the character of atomic

vacancy-induced fracture of the nanowire. For the atomic vacancies in a single-layer crystalline plane, maybe it is very difficult to attain in real applications. Moreover, there are also some difficulties for MD simulations in finding physical influences of atomic vacancy with average or random distributions. However, by our enough tests and comparisons, the constructed "a single atomic layer" could be helpful for offering insight into the deformation and fracture behavior of the nanowires under atomic vacancies.

For all MD calculations, the temperature was set at 300 K. Nośe-Hoover thermostat[27-29] was used as a rescaling method of velocity. With the method of Verlet list, the leapfrog algorithm was applied for the integration of motion equations to obtain velocity and trajectories of atoms with a time step of 1.6 *fs*.[10,11,30] Free boundary condition was adopted. All presented MD simulations and visualization processes were performed with the software NanoMD.[31] For potential functions, tight-binding molecular dynamics (TB-MD)[32,33] or Car-Parrinello molecular dynamics (CP-MD)[34] simulations could give relatively accurate results. However, these potential functions have some difficulties for so many calculations. In addition, the material density decreased with the tensile strain increasing, and the systems were in relative low-stress, not high-stress conditions. Therefore, embedded-atom method (EAM) developed by Johnson[35] might be the best choice for this particular purpose. In addition, a statistical analysis and a series of comparisons[36,37] may also reduce the systematic errors to ensure the reliability of MD simulations. The total energy was given by:

$$E = \frac{1}{2}\sum_{ij} V(r_{ij}) + \sum_{i} F(\rho_i), \quad (1)$$

$$\rho_i = \sum_{i \neq j} \varphi(r_{ij}) \quad (2)$$

where E is the total internal energy of the system, V is the pair potential between atoms i and j, and r_{ij} is the distance between them, $F(\rho_i)$ is the energy to embed atom i in an electron density ρ_i, $\varphi(r_{ij})$ is the electron density at atom i due to atom j as a function of the distance r_{ij}. The stress within the nanowire was computed by the Virial scheme,[38] and the overall stress was taken as the average of all atomistic stresses. The corresponding stress distributions along the tensile direction (z-direction) were averaged over atoms on the same xy-plane (in this work, the stress was averaged over a plane with a depth of one crystal constant in the z-direction, corresponding to about several thousand atoms at the initial state).[39] In the z direction, the corresponding atomic stress was expressed in terms of EAM potential functions as following:

$$\sigma_i^{zz} = \frac{1}{\Omega_i}\left\{-m_i v_i^z v_i^z + \frac{1}{2}\sum_{j \neq i}\left[\frac{\partial \phi}{\partial r_{ij}} + \left(\frac{\partial F}{\partial \rho_i} + \frac{\partial F}{\partial \rho_j}\right)\frac{\partial f}{\partial r_{ij}}\right]\frac{r_{ij}^z r_{ij}^z}{r_{ij}}\right\} \quad (3)$$

where σ_i^{zz} is the stress tensor of atoms α in the tensile direction (z-axis), Ω_i is the volume of i atoms, m is the mass, and v_i^z is the velocity component of atom i in the z direction. ϕ, F, ρ, f are parameters from EAM potential,[32] which corresponding to the pair potential, the embedded energy, the electron density between the atom i or j and all other atoms, the electron density in r_{ij} between atomic i and j, respectively. The first and second terms in the right side of the above equation represent the thermal effect and the atomic interactions respectively.

For the analysis of crystalline structure, the radial distribution function (RDF) was expressed as following,

$$g(r) = \frac{2V}{\mathrm{N}_m^{\,2}} \left\langle \sum_{i<j} (r - r_{ij}) \right\rangle \quad (4)$$

Based on this function, $\rho g(r)\mathrm{d}r$ means the probability of finding an atom in the volume element dr at a distance r from a given atom, and (in three dimensions) $4\pi\rho g(r)r^2\Delta r$ indicates the mean number of atoms in a shell of radius r and thickness dr surrounding the atom. Further detail calculation procedures were in accordance with the reference reported.[11]

3. Results and discussion

3.1 The breaking position distributions with different atomic vacancy ratios

The fracture of nanowires is very important for their utility in devices. If the breaking position is predictable, the nanowire can be strengthened near the breaking position. One case is not predictable for the fracture of the nanowire, while many cases will show a statistic feature. By statistical analysis, the histograms of the final breaking positions will reflect the relationship between the fracture of the nanowire and deformation mechanism induced by atomic fluctuation under the size effect. In a microscopic viewpoint, different nanowire sizes can result in different atomic fluctuations. The constructed atomic vacancies, as the typical "mechanical traps", could disturb the original ways of atomic movements, and the atomic vacancy ratio will reflect the fracture impact of atomic vacancy. For the position of atomic vacancy, our previous work[15,16] showed that one atomic vacancy with the ratio of 2% could

induce different breaking position distributions of nanowires ($5a \times 5a \times 15a$) with the change of atomic vacancy position. It was indicated that, whether the vacancy position changed or not, the tensile wave propagation was sensitive to slight atomic vacancy in the stretching process of the gold nanowire ($5a \times 5a \times 15a$). In this study, we also mainly considered the sensitivity of atomic vacancies on the deformation and fracture of nanowires. Thus, in order to compare effectively the breaking position distributions of the two sizes, a single layer of atomic vacancies was set in the middle of nanowires, which would definitely induce symmetric breaking of the gold nanowire in the middle.

Fig. 2(a) and 2(b) show statistical histograms of the final breaking positions of nanowires, and the influence of atomic vacancies on the fracture styles of nanowires with two different sizes by regulating atomic vacancy ratios. The histograms were fitted with Gaussian function, and the fitting peaks represented a most probable breaking position (MPBP) or MPBPs of nanowires. Fig. 2(a) shows breaking position distributions of [100] single-crystal gold nanowires (size I, $3a \times 3a \times 9a$) at different atomic vacancy ratios. The position of the single-layer atomic vacancies was fixed at 0.5 of the normalized length. Atomic vacancy ratios were set from 4% to 35%. Within the range of atomic vacancy-induced fracture, the MPBP was in the middle of the nanowire, and the fitting peaks were single peaks for all of the vacancy ratios. The width of the peaks firstly increased and then decreased with vacancy ratio increasing, which could be attributed to the deformation and fracture characters of nanowires for their micro-atomic fluctuation at different atomic vacancies and different tensile wave

propagations.[15,24,40,41] For the perfect nanowire with size I, the MPBP of the nanowire was at 0.5 of the normalized length. Under symmetrical stretching at two ends of the nanowire, the tensile wave propagated from two ends to the middle part, and the wave superposition brought about the increasing of atomic potential energy in the middle of the nanowire (part I at Fig. 2a). When the vacancy ratio increased from 0% to 4%, atomic vacancies disturbed the tensile wave propagation. As a result, the blocked wave induced its superposition at the region of atomic vacancies when symmetric stretching was applied on the nanowire (part II at Fig. 2a). In addition, one single layer of atomic vacancies was only set in the middle, which may resulted in the superposition of blocked waves in the middle of the gold nanowire (size I, $3a \times 3a \times 9a$). Under the double actions, the breaking position distribution appeared with peak width increasing and peak height decreasing at the vacancy ratio of 4%. Until the vacancy ratio increased to 25%, the wave propagation was hindered by atomic vacancies. The tensile wave was difficult to propagate from two ends to the middle, and a highly concentrated wave was observed (part III at Fig. 2a). So the breaking position distribution showed a high single peak under atomic vacancies.

For the [100] single-crystal gold nanowire with size II ($9a \times 9a \times 27a$) in Fig. 2(b), the breaking position distribution was divided into two parts when atomic vacancy ratio was fixed at 0%. The fracture of the nanowire ($9a \times 9a \times 27a$) dated from deformation mechanism exhibited ordered slippage of crystalline structure. The tensile wave superposition was mainly from symmetrical stretching at two ends of the nanowire (part I at Fig. 2b). Comparing with the distribution styles of size I ($3a \times 3a$

× 9*a*) and other previous work,[15,17] different distribution styles were usually from surface effect in nanowires with relatively small sizes. When a mechanical trap was constructed by atomic vacancies at size II (9*a* × 9*a* × 27*a*), slight atomic vacancies with the ratio of 0.6% have disturbed the tensile wave propagation. With the blocked waves, the wave superposition positions moved from two ends to the constructed atomic vacancies when symmetric stretching was applied to the gold nanowire. As the scheme shown in Fig. 2b (part II), the fracture of the nanowire was from actions of slippage and symmetric tension. With the vacancy ratio increasing, the MPBP in the corresponding breaking position distribution was gradually moving to the constructed atomic vacancy position. The MPBP was apt to distribute at the vacancy position at vacancy ratio of 15%. While the MPBP was completely stable at the vacancy position with vacancy ratio of 30%, indicating that the tensile wave propagation ended owing to atomic vacancies. Corresponding to the schematic diagram in Fig. 2b (part III), the atomic vacancies could dominate the fracture of the nanowire when the vacancy ratio was enough high.

The breaking position distributions not only reflected the relationship between macro-breaking characters of nanowires and micro-atomic fluctuations under atomic vacancies, but also exhibited the effect of surface atoms. For small system of nanowires (3*a* × 3*a* × 9*a*), surface atoms have played an important role in the deformation mechanism. The constructed atomic vacancies with little ratio were difficult to disturb the atomic movement styles, showing insensitivity of atomic vacancies to the breaking position distribution. When the nanowire size increased to

($5a \times 5a \times 15a$),[15] one atomic vacancy could affect atom movements in an equilibrium state and the corresponding wave propagation, indicating the sensitivity of atomic vacancies. For the nanowire sizes of ($9a \times 9a \times 27a$), bulk atoms have dominated the atomic movement styles. As a result, one atomic vacancy could also disturb the tensile wave propagation. The double actions have improved the sensitivity of atomic vacancies to the breaking position distributions. These characters indicated that there would be a competition between the movements of bulk atoms and surface atoms in the tensile deformation of gold nanowires under size effect. Our previous work,[15-17] have demonstrated that the MPBP was not uniform in the middle region of distribution. With size effect, the MPBP would transfer from the middle to two ends. Between ($3a \times 3a \times 9a$) and ($9a \times 9a \times 27a$), there should be a transition size such as ($8a \times 8a \times 24a$) in the breaking position distributions of gold nanowires. In addition, the tensile rate was also important for the deformation and fracture of the gold nanowire. Especially for the region of high strain rates, the behavior of the nanowire would be different under different strain rate conditions.[15,26] However, for the selected strain rate of 1.0% ps^{-1} in this study, the tensile deformation could be considered as quasi-static state of the gold nanowire, and such a low strain rate could avoid the strain rate effect as much as possible. Thus, for the sizes of ($3a \times 3a \times 9a$) and ($9a \times 9a \times 27a$), we could believe that size effect dominated the deformation and fracture behaviors of gold nanowires. The relevant work was in progress.

3.2 The deformation mechanism with different atomic vacancy ratios

The fracture character of the nanowire from the deformation mechanism under size effect, is affected by atomic vacancies. As shown in Fig. 3(a), (see Supplementary Video S1), there was no obvious slippage plane for size I of nanowire during the whole tensile deformation. After the first yield state <2>, the nanowire undergone an irreversible structural rearrangement to a disordered cluster configuration at the state <3>, and the obvious amorphous structure was found at <3-A>. Upon further stretching, the reconstructed amorphous structure obtained after elastic deformation was not able to attain the minimum energy state and hence a breaking neck appeared along the middle region of the nanowire. With the tensile strain increasing, a cluster (see the state <6-B>) exhibited around the breaking tip at <6>, and then the overall rupture happened in the middle of the gold nanowire. Comparing with size I of nanowire, the obvious difference was the appearance of the slippage plane for size II of nanowire. In Fig 3(b), (see Supplementary Video S2), the nanowire undergone slippage along (111) plane at the state <3>, (see <3-A>). For a closed pack structure such as FCC, the existence of the smallest Burgers vectors made it energetically favorable to reconstruct along the (111) slippage planes. With strain increasing, obvious slippage planes appeared in the whole nanowire, which accorded with the slippage mechanism that proposed by Finbow *et al*..[30] Along the slippage planes, there were some relatively ordered crystalline structures during the whole deformation of the nanowire, and only slight amorphization structures appeared at the two ends of the nanowire. Upon further stretching, three breaking necks appeared at the state <6>, and

the fracture of the nanowire was observed at one end under symmetric tensile action firstly. From <7-B>, we could find some twinned crystalline structures around the breaking neck, and the nanowire still retained the relatively ordered structure. Based on the above analysis, the rupture styles of nanowires under different sizes could be that, nanowires with small size would like to show disordered cluster rupture, and the large-sized nanowires were apt to result in ordered slippage rupture, which could be attributed to surface atom effects. In the view of crystalline, the influence of sizes on nanowire rupture could be illustrated with the radial distribution function (RDF). As shown in Fig. 3(c) and 3(d), the peaks of RDF curves were both sharp at the beginning of tensile, indicating the retained perfect crystalline structures of gold nanowires after relaxation states. After that, the peak height at size II of nanowire decreased in the nearest neighbor distance, but the peaks still kept sharp features. It could be concluded that the nanowire could maintain good crystalline structures easily at size II. In contrast, the peaks of RDF at size I of nanowire were broadened and rough at the nearest neighbor distance, and the heights of the peaks reduced obviously in the whole tensile process of the nanowire, which could be attributed to acute atomic movement of the nanowire with small size.

For the investigation about atomic vacancies, atomic vacancies were constructed in a single-layer crystalline plane of nanowires to study its sensitivity to the deformation style. For size I of nanowire, Fig. 4(a) and 4(b) showed the representative deformation and breaking processes of nanowires with vacancy ratios of 4% and 35%, respectively. As shown in Fig. 4(a), (see Supplementary Video S3), the atomic

vacancy ratio was 4%, and one atomic vacancy could induce the disordered crystalline structure around the region of atomic vacancy. However, the disordered degree was not obvious at <3-A>. In comparison with the perfect nanowire at Fig. 3(a), a cluster band appeared and became longer at its breaking tip of <6-B>. With the tensile strain increasing, the gold nanowire broke in the middle part. From Fig. 4(b), (see Supplementary Video S4), the disordered crystalline structure (<3-A>) appeared obviously around the plane of atomic vacancies when the atomic vacancy ratio increased to 35%. With the strain increasing, the breaking neck appeared in the middle of the nanowire. Under the effect of atomic vacancies, the nanowire broke obviously in the middle of the vacancy crystalline plane, while retained good crystalline structure at the two ends. For size II of nanowire at Fig. 4(c), the corresponding Video S5 (see Supplementary Video S5) showed that slippage planes did not appear when one atomic vacancy with the ratio of 0.6% was in the single-layer crystalline plane of the nanowire. After the elastic deformation, only a few slippage planes (<3-A>) were observed in the middle region. With local amorphization, some twisted crystalline planes appeared in the plastic deformation process. In comparison with the perfect nanowire (Fig. 3(b) and Video S2), the breaking neck was only one, and the nanowire broke around the middle region with the stretching strain increasing. It could be deduced that mechanical trap induced by one atomic vacancy had hindered the appearance of slippage plane. With uniaxial stretching, the atomic vacancy resulted in the twisted crystal planes and some disordered crystalline structures. When the vacancy ratio increased to 30% at Fig. 4(d), the whole deformation of the

nanowire was in a brittle way with the reduced ductility (see Supplementary Video S6). From the state <3-A> of Fig. 4(d), we could also find that the disordered structure mainly formed around the plane of atomic vacancies. With strain increasing, the brittle rupture happened at the atomic vacancy position of the nanowire.

The above deformation characters have shown that both of small systems and atomic vacancies could facilitate the appearances of disordered crystalline structures during the uniaxial stretching. This could be attributed to atomic vacancies and surface atoms belonging to imperfect atoms. In comparison with block atoms, imperfect atoms have higher potential energies. In the tensile deformation, the increasing potential energy is from the breaking of atomic bonds. The bond breaking is a direct consequence of atomic vibration overcoming the interatomic cohesive energy, which in turn causes the disordered crystalline structure. Here, the degree of lattice order was also evaluated by the maximum average potential energy per atom in the tensile deformation process of the nanowire, which replaced the damaged value of the system induced by uniaxial tension. As shown in Fig. 5, the maximum average potential energy per atom increased both in two different sizes of nanowires when the atomic vacancies were constructed at single-layer crystalline planes. The increasing value of potential energy ($\Delta E1$) was set as 0.061 eV for size I ($3a \times 3a \times 9a$) from the vacancy ratio of 0% to 4%. $\Delta E2$ was set as 0.030 eV for size II ($9a \times 9a \times 27a$) from the vacancy ratio of 0% to 0.6%, and the ratios of 4% and 0.6% both have one atomic vacancy in the single-layer crystalline plane for two different sizes. Comparing with two different sizes at the vacancy ratio of 0%, the potential energy of size I was

higher than that of size II, with the increasing of potential energy (ΔE) 0.066 eV. Whether there were atomic vacancies or not, the decreasing of the nanowire size with the same aspect ratio always brought the increasing of potential energy. This indicated that the increasing of potential energy mainly resulted from surface atoms, and the atomic vacancy exhibited little influence on the potential energy. For surface atoms were typical imperfect atoms that had high potential energies, the ratio of the surface atoms to all atoms decreased with nanowire size increasing. A comprehensive understanding of deformation mechanism was that the surface atoms at small size could induce the disordered crystalline structures and the nanowire belonged to a disordered cluster rupture. Meanwhile, atomic vacancies with little ratio had given the appearance of a cluster band at the fracture of the nanowire. For the large size of nanowires, slippage maintained good crystalline structure during the tensile deformation of the nanowire. The constructed atomic vacancies could hinder slippage. For the two different sizes of nanowires, if there were enough large vacancy ratios, the constructed atomic vacancies not only could determine the fracture of nanowires, but also could maintain relative good crystal structures.

3.3 The mechanical properties with different atomic vacancy ratios

The effect of atomic vacancies on atom movement of the nanowire could be reflected by the deformation mechanism and fracture character of the nanowire. For the relevant analysis of mechanical property, the stress-strain response could give an insight into the mechanical failure and operation behaviors of nanoscale devices. As shown in Fig. 6(a), the typical stress-strain responses were selected for the [100]

single-crystal gold nanowires with two different sizes, which were ($3a \times 3a \times 9a$, size I) and ($9a \times 9a \times 27a$, size II). The strain (ε) was defined as $\varepsilon = (l - l_0)/l_0$, where l was the current stretching length and l_0 was the length just after relaxation. The stress (σ) in the tensile direction was calculated by the Virial scheme,[33] and it was obtained by averaging the ones of all the atoms in *xy*-plane, not for a specific atom in the nanowire. In Fig. 6(a), stress increased linearly with the strain increasing at the beginning, in accordance with the elastic deformation of the nanowire. The stresses at the first yield points corresponded to the deformation behaviors were shown at <2> of Fig. 3(a) and 3(b), respectively. After the first yield point, the stress decreased abruptly indicating a beginning of an irreversible plastic deformation of the nanowire. Subsequently, yield cycle repeated with stress decreasing, implying the presence of temporary stable states in the tensile processes of nanowires. When the nanowire could not reconstruct and maintain a stable state under the tensile action, the yield cycle was over, corresponding to the behaviors at <7> of Fig. 3(a) and 3(b), respectively. During the whole yielding cycle, the periodicity vibrations of the stress-strain responses presented in both nanowire sizes, and the stress-strain curve was relatively smooth for size II. In contrast, the stress was scattered and vibrated acutely with a large amplitude at size I. This indicated that small nanowire size could induce the crystal lattice of size I vibrate acutely at their equilibrium position under symmetric tension with the same strain rate, and the atoms with large atomic entropy could not be in a low energy state, so the stress of size I tended to fluctuate with a large amplitude. After the initial yield point, size II has exhibited a stress plateau,

which extended for about 80% strain with the stress of about 3.0 GPa. The longer stress plateau of size II leaded to a larger fracture strain, which corresponded to a larger ductility of the nanowire, because of the slippage-dominated behavior of the nanowire. The stress plateau of size I was small with the fluctuating stress, leading to small fracture strain. The difference in the stress plateau magnitude was rooted in different deformation mechanisms: the large stress plateau for size II was formed by the relative ordered atom movement with a few slippage planes; while the small stress plateau for size I was due to some disordered atom movement with obvious surface effect. For the first yield point, the first yield stress of size I was larger than that of size II, while the first yield strain of size II was obviously larger than that of size I. The result demonstrated that size I was easy to be in plastic deformation with high yield stress, which resulted from the surface effect on the deformation behavior of the nanowire with small size. Whereas, slippage mechanism dominated the deformation of size II, inducing the large ductility of the nanowire with large fracture strain.

For the first yield properties of nanowires under atomic vacancies, Fig. 6(b)-6(d) gave the first yield strain, the first yield stress and Young's modulus against vacancy ratios at two different sizes, respectively. The average statistical results are from 300 samples for each condition. In Fig. 6(b), the first yield strain of size I fluctuated around the range from 0.030 to 0.055 within atomic vacancy ratio, attributing to the deformation stability of the nanowire induced by surface effect of small size. In contrast, the first yield strain increased with atom vacancy ratio increasing for size II, with increasing value of the first yield strain ($\Delta N1$) being 0.005 and atomic vacancy

ratio from 0% to 0.6%. The increasing of size had improved the first yield strain, the value of which from size I was 0.035 higher than that of size II. It was difficult for size I to maintain elastic deformation, because the surface atom effect from small size could easily induce the deformation instability of the nanowire. For the influence of atomic vacancies, the large proportion of surface atom could also result in the instability of the first yield strain for size I. For the first yield stress against atomic vacancy ratio at two different sizes, the yield stress at size I was uncertain with large errors. The reason might be that the surface atoms had occupied an important place, inducing the stress instability. So the influence of atomic vacancy was unobvious at size I. For size II, the increasing value of the first yield stress ($\Delta S1$) was 2.5 GPa from atomic vacancy ratio of 0% to 0.6%, from which we observed that the first yield stress decreased with the ratio increasing. The stress character corresponded to the deformation mechanism, one atomic vacancy could hinder the appearance of slippage plane, and the increasing of disordered crystalline structure had strengthened the stress. Therefore, it could be concluded that atomic vacancies could obviously affect the atomic microstructure in the deformation process of the nanowire. However, the decreasing of yield stress with vacancy ratio increasing might result in the atomic vacancy-induced fracture of nanowires. The stress at size I was mainly from surface atoms, which determined the elastic and plastic deformation behavior of the nanowire. Fig. 6(d) showed Young's modulus against atomic vacancy ratio. Comparing with the perfect single-crystal gold nanowires, atomic vacancies have improved Young's modulus for nanowires with two sizes. For size I, Young's modulus increased firstly

and then decreased with vacancy ratio increasing. However, the influence of atomic vacancy ratio was not obvious for size II. The mechanical strength of nanowires could be evaluated by Young's modulus, which was related with the first yield strain. The beginning of plastic deformation could directly affect Young's modulus of the nanowire. For the mechanical strength of the nanowire, low atomic vacancy ratio could always give the increasing of mechanical strength, because of the surface atoms belonging to under-coordinated atoms and the atomic coordination imperfection generated by atomic vacancies, both of which could increase the bond strength. It was consistent with a bond-order-length-strength correlation mechanism proposed by Sun[42] that atomic coordination imperfection could cause the remaining atomic bonds to contract spontaneously associated with bond strength. Pauling[43] and Goldschmidt[44] also indicated that the atomic coordination number reduction could cause shrinkage of atomic size, or the contraction of the remaining bonds, inducing an increase in strength of metallic atom bonds. In addition, it was unstable for the first yield stress and Young's modulus of size I within the atomic vacancy ratios, attributing to the double actions of small size and the uniaxial tensile atomic movements. For the former action of small size, surface atoms distributed in small systems and under-coordinated atoms were located at the surface. During the relaxation to the initial energy minimization, the relaxed structure with relatively high potential energy could not preserve the stable elastic deformation of the nanowire. For the latter action of the uniaxial tensile atomic movement, the randomness of metallic atoms was enhanced in the uniaxial tensile process of the nanowire with small size, inducing the

instability of mechanical strength. However, this action was within the limitation of atomic vacancy-induced fracture of the nanowire.

4. Conclusion

In summary, the fracture, deformation mechanism and mechanical properties of gold nanowires were studied by MD simulations. The ratios of atomic vacancies were set from 4% to 35% for size I of gold nanowire ($3a \times 3a \times 9a$) and from 0.6% to 30% for size II of gold nanowire ($9a \times 9a \times 27a$). It was observed that: (1) two gold nanowire sizes exhibited two different fracture styles induced by unaxial tension. For size I, the MPBP of the gold nanowire was in the middle region, while the MPBP distributed at the two ends for size II. For the same positions of single-layer atomic vacancies, the influence of vacancy exhibited more obviously for size II than that for size I. (2) The deformation mechanisms of two different nanowire sizes were different, the small-sized gold nanowire showed a disordered cluster rupture, while the large-sized gold nanowire exhibited an ordered slippage rupture. The appearance of atomic vacancies could induce the cluster band at the breaking point of size I. To some certain, the atomic vacancies could also hinder the slippage planes of size II. (3) The mechanical strength of gold nanowires decreased with size increasing.

Acknowledgments

This project was supported by the National Natural Science Foundation of China (Grant No. 51406074), China Postdoctoral Science Foundation Funded Project (2012M521290), Special Postdoctoral Science Foundation funded project of Jiangxi Province, Scientific Research Fund of Jiangxi Provincial Education Department (GJJ14201), the National Natural Science Foundation of China (Grant No. 21273113), the Foundation for Innovative Research Groups of the National Natural Science Foundation of China (Grant No. 21121091), and National Key Technology R&D Program of China (Grant No. 2012BAF03B05).

References

[1]K. L. Ekinci, and M. L. Roukes, Rev. Sci. Instrum., 2005, **76**, 061101.

[2]J. J. Kruzic, Science, 2009, **325**, 156.

[3]C. M. Lieber, MRS Bull, 2003, **28**, 486.

[4]K. J. Hemker, Science, 2004, **304**, 221.

[5]P. L. Gai, and M. A. Harmer, Nano Lett., 2002, **2**, 771.

[6]L. L. Hu, L. X. Huo, J. Q. Zhou, Y. Wang, and S. Zhang, J. Nanopart. Res., 2012, **14**, 677.

[7]N. Agrait, J. G. Rodrigo, C. Sirvent, and S. Vieira, Phys. Rev. B, 1993, **48**, 8499.

[8]M. Tsutsui, T. Ohshiro, K. Matsubara, M. Furuhashi, M. Taniguchi, and T. Kawai, J. Appl. Phys., 2010, **108**, 064312.

[9]I. K. Yanson, O. I. Shklyarevskii, S. Csonka, H. van Kempen, S. Speller, A.I. Yanson, and J.M. van Ruitenbeek, Phys. Rev. Lett., 2005, **95**, 256806.

[10]M. P. Allen, and D. J. Tildesley, Computer Simulation of Liquids (Clarendon, New York, 1997).

[11]D. C. Rapaport, The Art of Molecular Dynamics Simulation, 2nd ed. (Cambridge University Press, Cambridge, UK, 2004).

[12]J. K. Diao, K. Gall, and M. L. Dunn, Nature Mater., 2003, **2**, 656.

[13]C. Deng, and F. Sansoz, Acs Nano, 2009, **3**, 3001.

[14]E. Z. da Silva, F. D. Novaes, A. J. R. da Silva, and A. Fazzio, Phys. Rev. B, 2004, **69**, 115411.

[15]F. Wang, Y. Gao, T. Zhu, and J. Zhao, Nanoscale, 2011, **3**, 1624.

[16]F. Wang, T. Chen, T. Zhu, Y. Gao, and J. Zhao, J. Appl. Phys., 2011, **110**, 084307.

[17]F. Wang, W. Sun, H. Wang, J. Zhao, M. Kiguchi, and C. Sun, J. Nanopart. Res., 2012, **14**, 1082.

[18]D. Wang, J. Zhao, S. Hu, X. Yin, S. Liang, Y. Liu, and S. Deng, Nano Lett., 2007, **7**, 1208.

[19]P. Reddy, S. Y. Jang, R. A. Segalman, and A. Majumdar, Science, 2007, **315,** 1568.

[20]B. Q. Xu, and N. J. J. J. Tao, Science, 2003, **301**, 1221.

[21]Z. Li, S. Shao, N. Li, K. McCall, J. Wang, and S. X. Zhang, Nano Lett., 2013,**13**, 5443.

[22]H. Zheng, A. Cao, C. R. Weinberger, J. Huang, K. Du, J. Wang, Y. Ma, Y. Xia, and S. Mao, Nat. Comm., 2010, **1**, 144.

[23]Y. Liu, J. Zhao, and F. Wang, Phys. Rev. B, 2009, **80**, 115417.

[24]F. Wang, Y. Liu, T. Zhu, Y. Gao, and J. Zhao, Nanoscale, 2010, **2**, 2812.

[25]F. Wang, W. Sun, Y. Gao, Y. Liu, J. Zhao, and C. Sun, Comput. Mater. Sci. 2013, 67, 182.

[26]F. Wang, Y. Gao, T. Zhu, and J. Zhao, Nanoscale Res. Lett., 2011, **6**, 291.

[27]S. Nośe, Mol. Phys., 1984, **52**, 255.

[28]S. Nośe, J. Chem. Phys., 1984, **81**, 511.

[29]W. G. Hoover, Phys. Rev. A, 1985, **31**, 1695.

[30]G. M. Finbow, R. M. LyndenBell, and I. R. McDonald, Mol. Phys., 1997, **92**, 705.

[31]J. Zhao, X. Yin, S. Liang, Y. Liu, D. Wang, S. Deng, and J. Hou, Chem. Res. Chin. Univ., 2008, **24**, 367.

[32]M. J. Mehl, and D. A. Papaconstantopoulos, Phys. Rev. B, 1996, **54**, 4519.

[33]E. Z. da Silva, A. J. R. da Silva, and A. Fazzio, Phys. Rev. Lett., 2001, **87**, 256102.

[34]J. Hutter, and A. Curioni, Chemphyschem, 2005, **6**, 1788 (2005).

[35]R. A. Johnson, Phys. Rev. B, 1989, **39,** 12554.

[36]J. Zhao, K. Murakoshi, X. Yin, M. Kiguchi, Y. Guo, N. Wang, S. Liang and H. Liu, J. Phys. Chem. C, 2008, **112**, 20088.

[37]L. Jiang, X. Yin, J. Zhao, H. Liu, Y. Liu, F. Wang and J. Zhu, J. Phys. Chem. C, 2009, **113**, 20193.

[38]H. Wu, Eur. J. Mech. a-Solids, 2006, **25**, 370.

[39]F. Wang, Y. Liu, X. Yin, N. Wang, D. Wang, Y. Gao, and J. Zhao, J. Appl. Phys., 2010, **108**, 074311.

[40]E. M. Bringa, J. U. Cazamias, P. Erhart, J. Stolken, N. Tanushev, B. D. Wirth, R. E. Rudd, and M. J. Caturla, J. Appl. Phys., 2004, **96**, 3793.

[41]B. L. Holian, Phys. Rev. A, 1988, **37**, 2562.

[42]C. Sun, Prog. Solid State Chem., 2007, **35**, 1.

[43]L. Pauling, J. Am. Chem. Soc., 1947, **69**, 542.

[44]V. M. Goldschmidt, Ber. Deut. Chem. Ges., 1927, **60**, 1263.

Table 1 The simulation conditions of the nanowire

Nos.	<1>	<2>	<3>	<4>	<5>	<6>	<7>
Ratio ($3a \times 3a \times 9a$)	4%	10%	15%	20%	25%	30%	35%
Ratio ($9a \times 9a \times 27a$)	0.6%	4%	10%	15%	20%	25%	30%

(*a* stands for lattice constant, 0.408 nm for gold.)

Figure Captions

Figure 1 Schematic illustration of theoretical models.

(a) Schematic illustration of the rupture of the single-crystal gold nanowire at the effects of size and atomic vacancies. In part I, the sizes of gold nanowires are ($3a \times 3a \times 9a$) and ($9a \times 9a \times 27a$), respectively, (a stands for lattice constant, 0.408 nm for gold). The symmetric tension is in z-direction. In part II, the rupture characters show size effects on the deformation behaviors of gold nanowires. In part III, the rupture characters show atomic vacancy effects on the deformation behaviors of gold nanowires, and the positions of atomic vacancies both distribute in the middle of nanowires. (b) Schematic illustration of the single-layer atomic vacancy distribution of size I ($3a \times 3a \times 9a$); (c) Schematic illustration of the single-layer atomic vacancy distribution of size II ($9a \times 9a \times 27a$). Atoms in white replace atomic vacancies.

Figure 2 The breaking position distributions of the [100] single-crystal gold nanowires.

(a) The breaking position distributions of nanowires with the atomic vacancy ratio from 4% to 35% at size I ($3a \times 3a \times 9a$); (b) The breaking position distributions of nanowires with the atomic vacancy ratio from 0.6% to 30% at size II ($9a \times 9a \times 27a$). (The dash lines are the constructed defect positions. Parts I, II, and III correspond to schematic illustrations about the tensile wave propagations of nanowires.)

Figure 3 The deformation behavior of the nanowire and the corresponding radial distribution function (RDF) at two sizes.

(a) The deformation behavior at size I of ($3a \times 3a \times 9a$); (b) The deformation behavior at size II of ($9a \times 9a \times 27a$); (<1> - <7> are the selected deformation characters; <3-A>, and <6-B> or <7-B> are the relevant amplified characters). RDF (c) at size I of ($3a \times 3a \times 9a$) and (d) at size II of ($9a \times 9a \times 27a$), respectively. (<1>, <2>, and <3> replace the beginning of stretching, the critical point between elastic and plastic deformation, and the breaking point, respectively. The "a_0" in horizontal axis means lattice constant, and 0.408 nm for gold.)

Figure 4 The deformation behavior of the nanowire under atomic vacancies.

(a) The size I of ($3a \times 3a \times 9a$) with the atomic vacancy ratio of 4%; (b) The size I of ($3a \times 3a \times 9a$) with the atomic vacancy ratio of 35%; (c) The size II of ($9a \times 9a \times 27a$) with the atomic vacancy ratio of 0.6%; (d) The size II of ($9a \times 9a \times 27a$) with the atomic vacancy ratio of 30%. (<1> - <7> are the selected deformation characters; <3-A>, and <6-B> are the relevant amplified characters).

Figure 5 The maximum average potential energy per atom of the [100] single-crystal gold nanowire plotted against atomic vacancy ratio at two different sizes.

(The maximum average potential energy per atom is obtained by averaging 300 values of calculated maximum potential energy of the atom, and the error bar indicates the average deviation of the average value calculated by the 300 values.)

Figure 6 The mechanical behaviors of the [100] single-crystal gold nanowires

(a) The representative stress-strain relationship of the nanowire at two different sizes; (b) The first yield strain of the nanowire plotted against atomic vacancy ratio at two different sizes; (c) The first yield stress plotted against atomic vacancy ratio at two different sizes; (d) Young's modulus plotted against atomic vacancy ratio at two different sizes. (The ratios are from 4% to 35% at size I of ($3a \times 3a \times 9a$), and are from 0.6% to 30% at size II of ($9a \times 9a \times 27a$), respectively.)

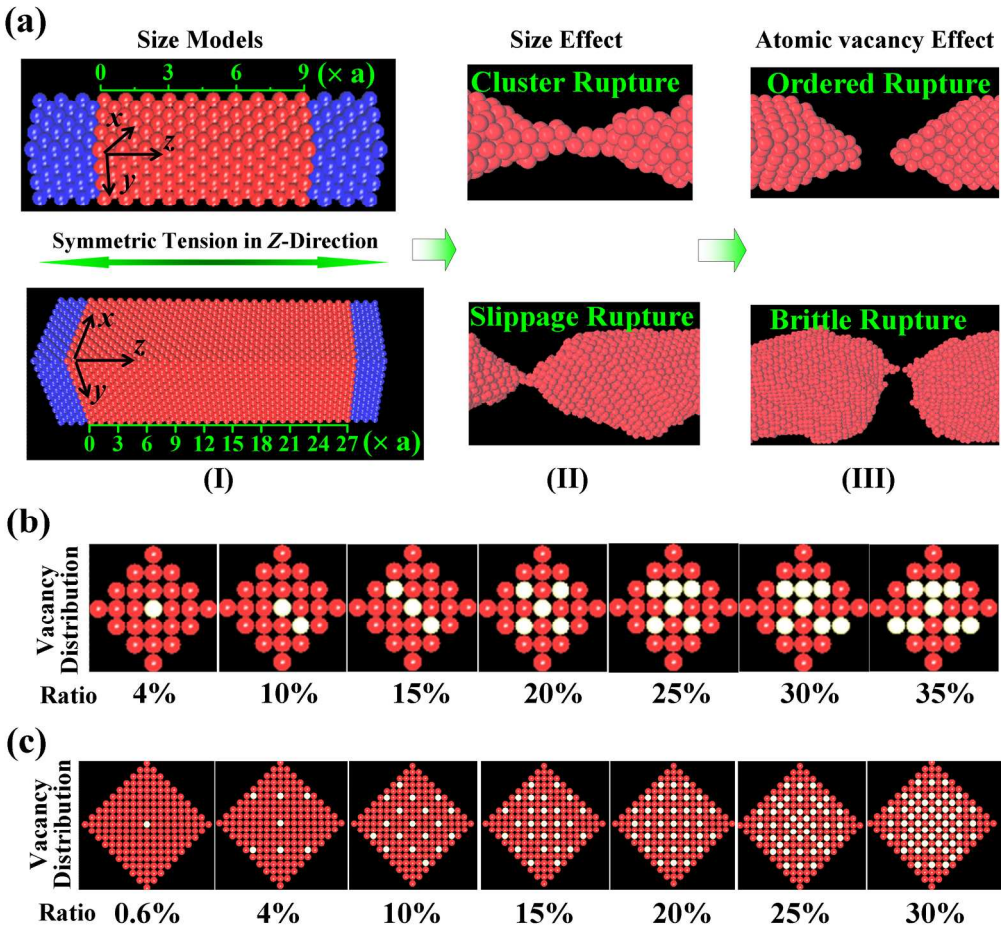

Schematic illustration of theoretical models.
117x109mm (600 x 600 DPI)

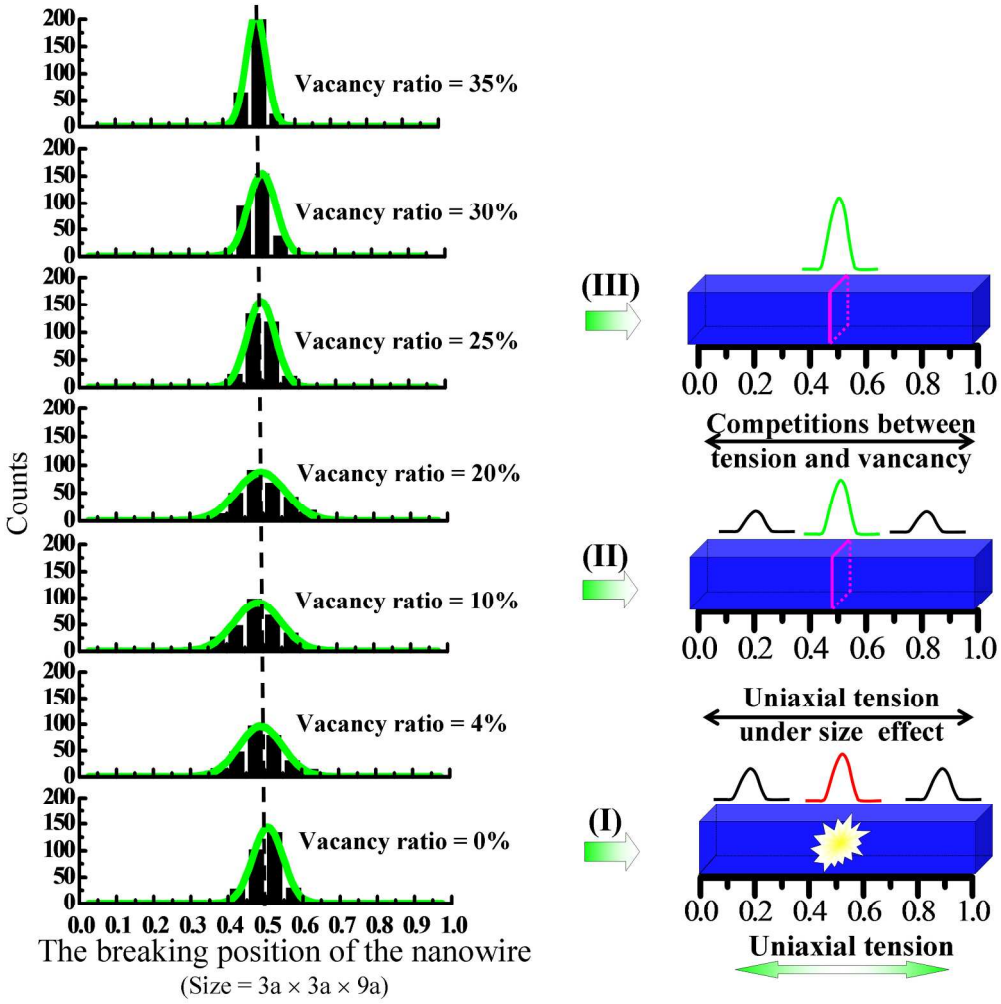

The breaking position distributions of the [100] single-crystal gold nanowires.
125x125mm (600 x 600 DPI)

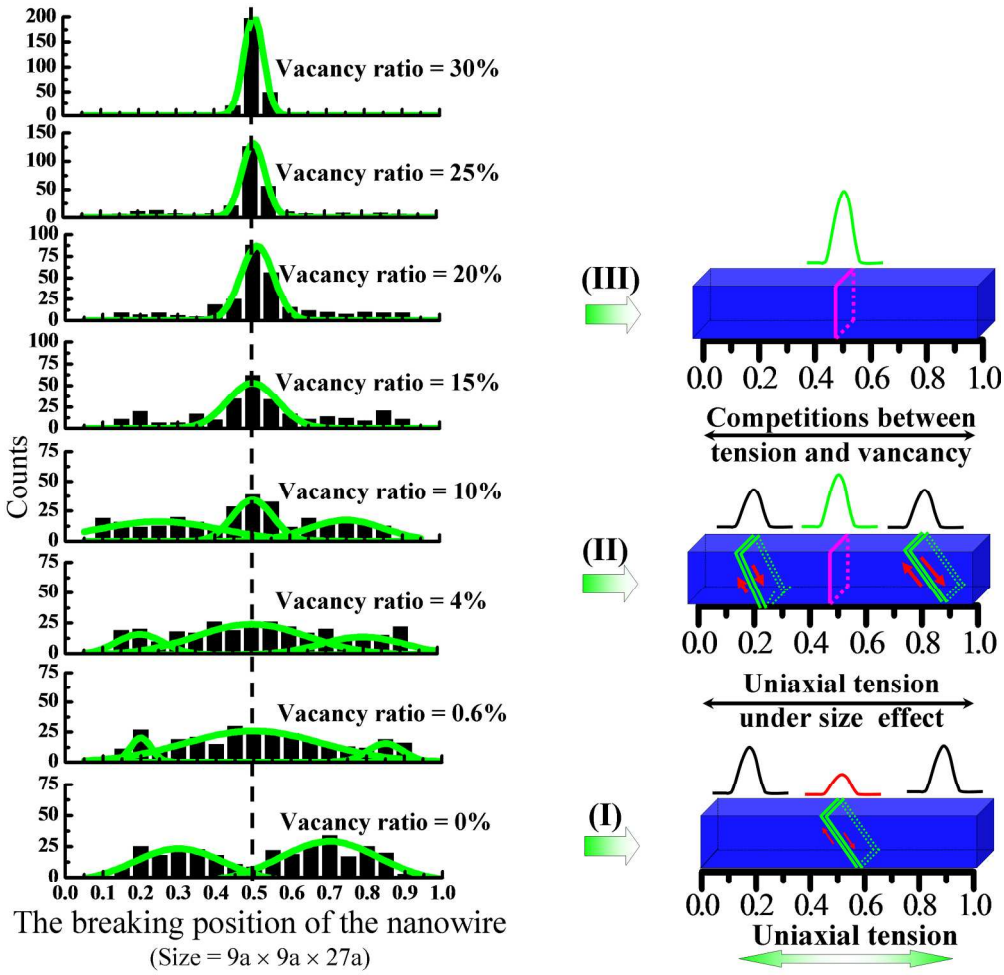

The breaking position distributions of the [100] single-crystal gold nanowires.
121x118mm (600 x 600 DPI)

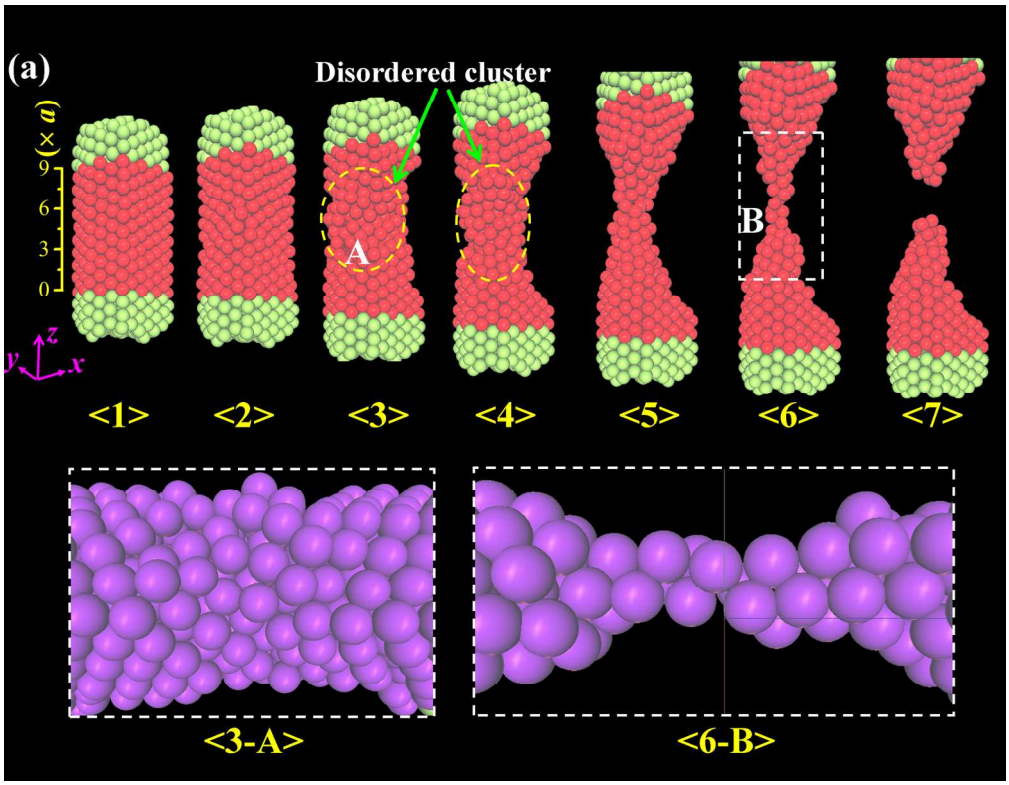

The deformation behavior at size I
96x75mm (600 x 600 DPI)

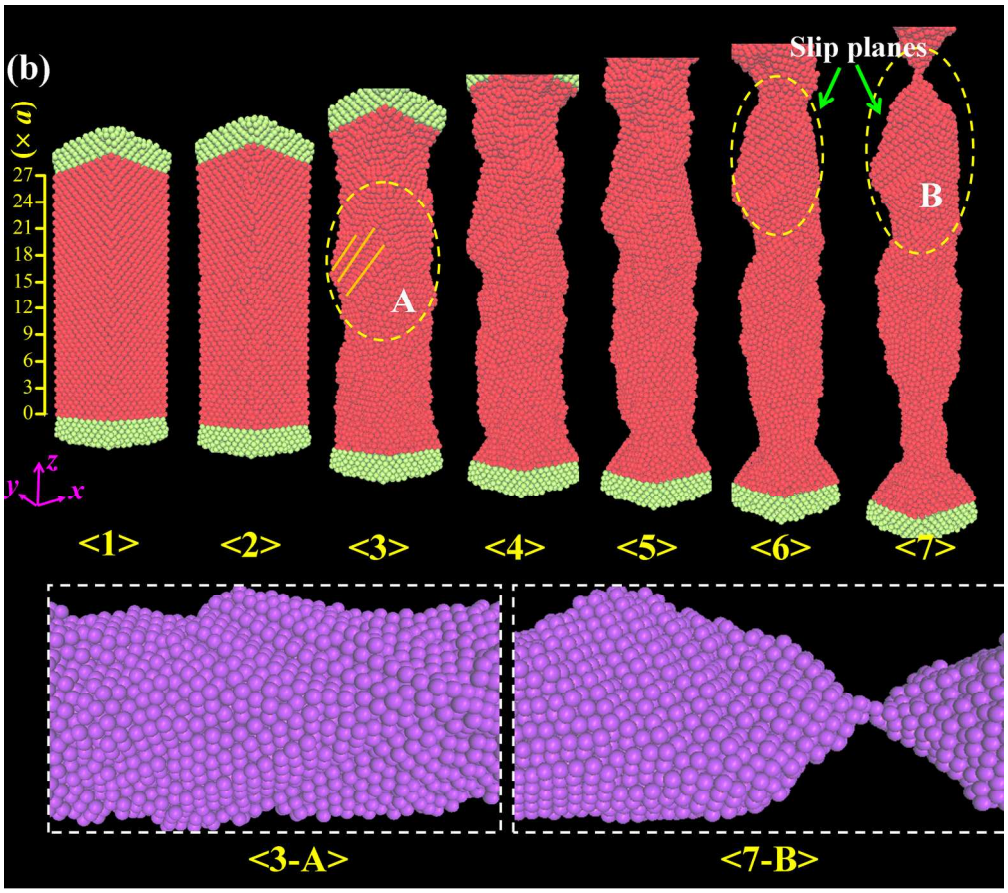

The deformation behavior at size II
103x91mm (600 x 600 DPI)

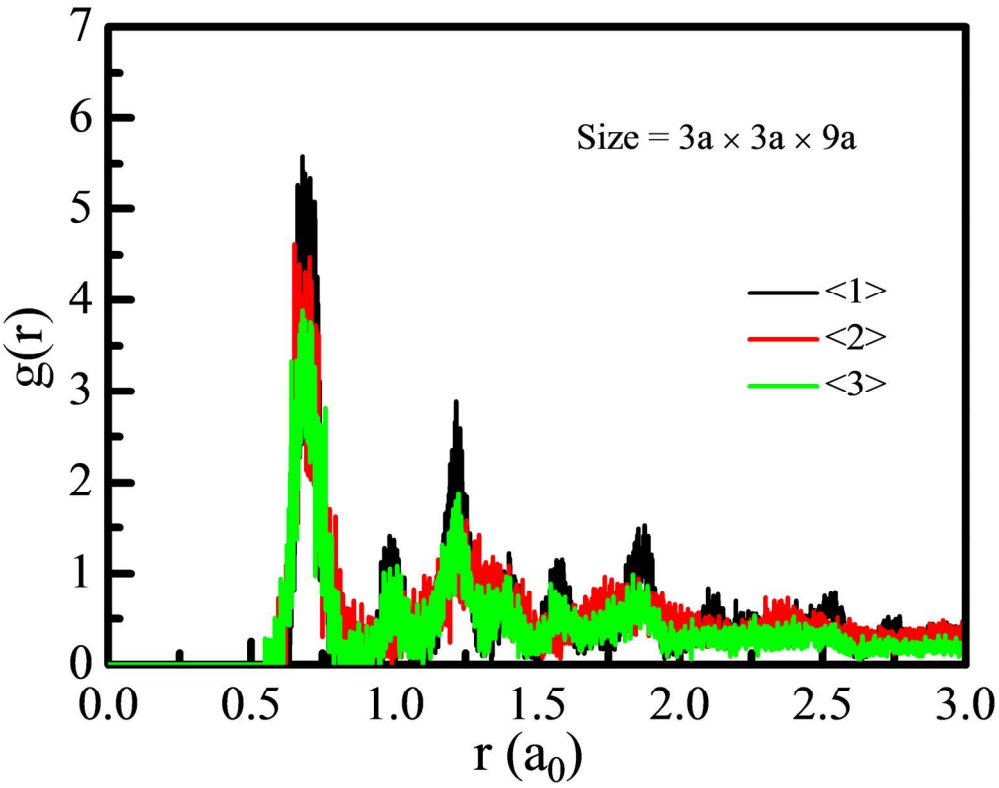

RDF at size I.
99x78mm (600 x 600 DPI)

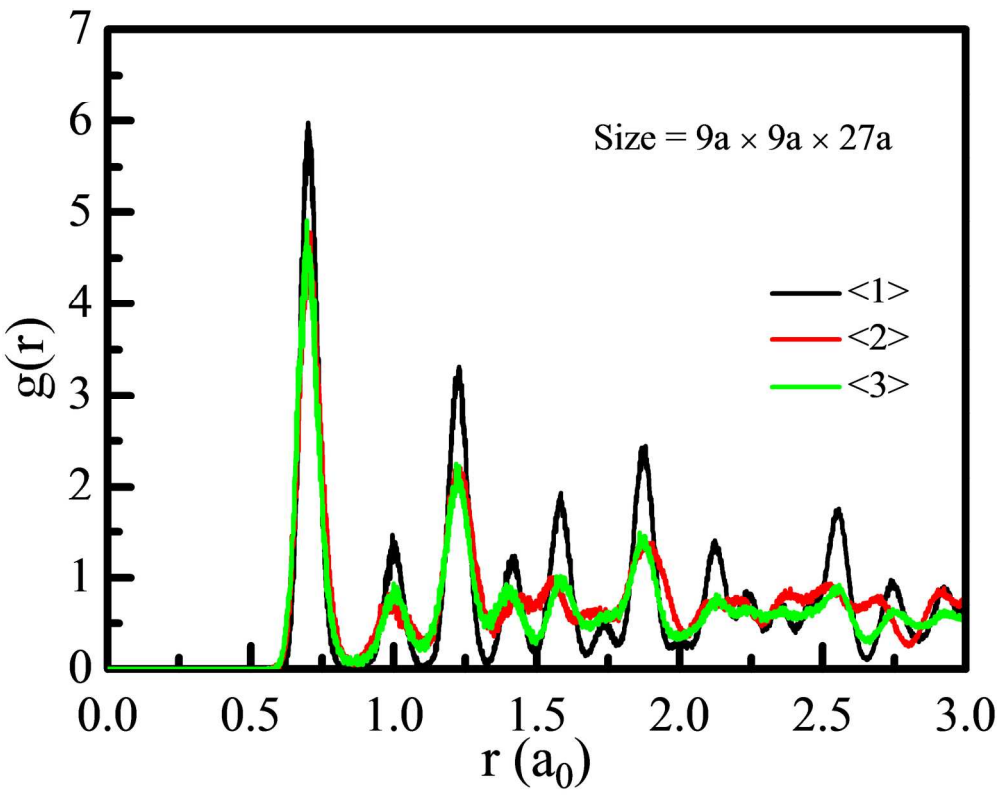

RDF at size II.
98x78mm (600 x 600 DPI)

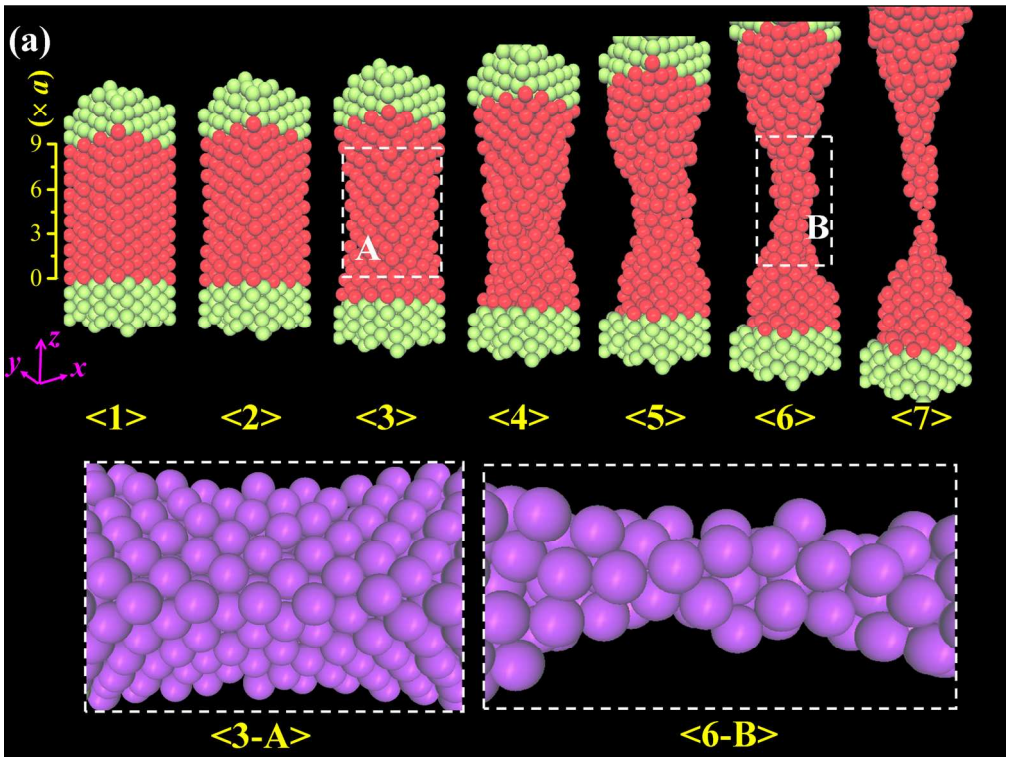

The deformation behavior of the nanowire under atomic vacancies.
93x70mm (600 x 600 DPI)

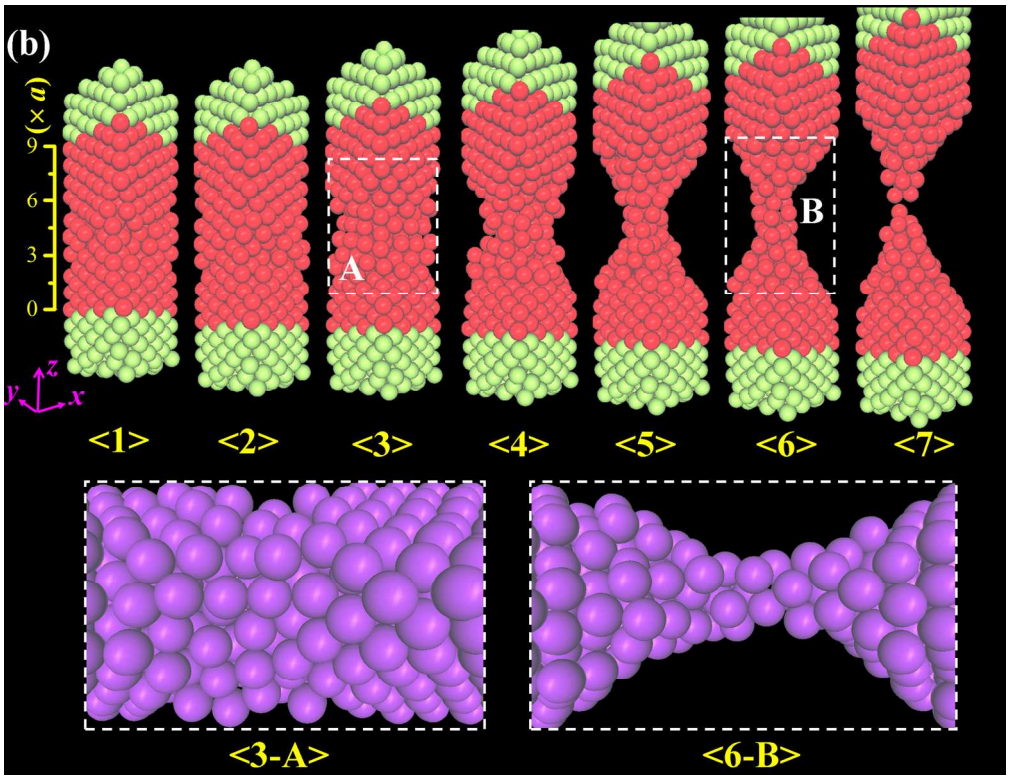

The deformation behavior of the nanowire under atomic vacancies.
96x73mm (600 x 600 DPI)

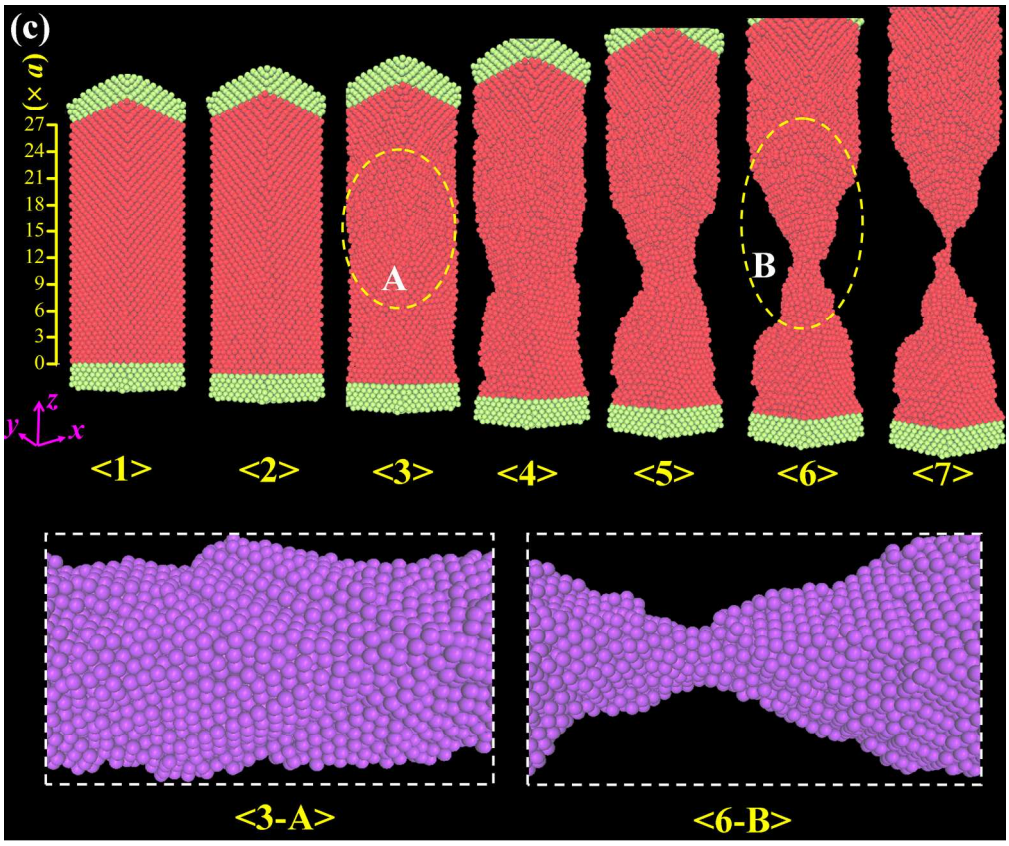

The deformation behavior of the nanowire under atomic vacancies.
104x87mm (600 x 600 DPI)

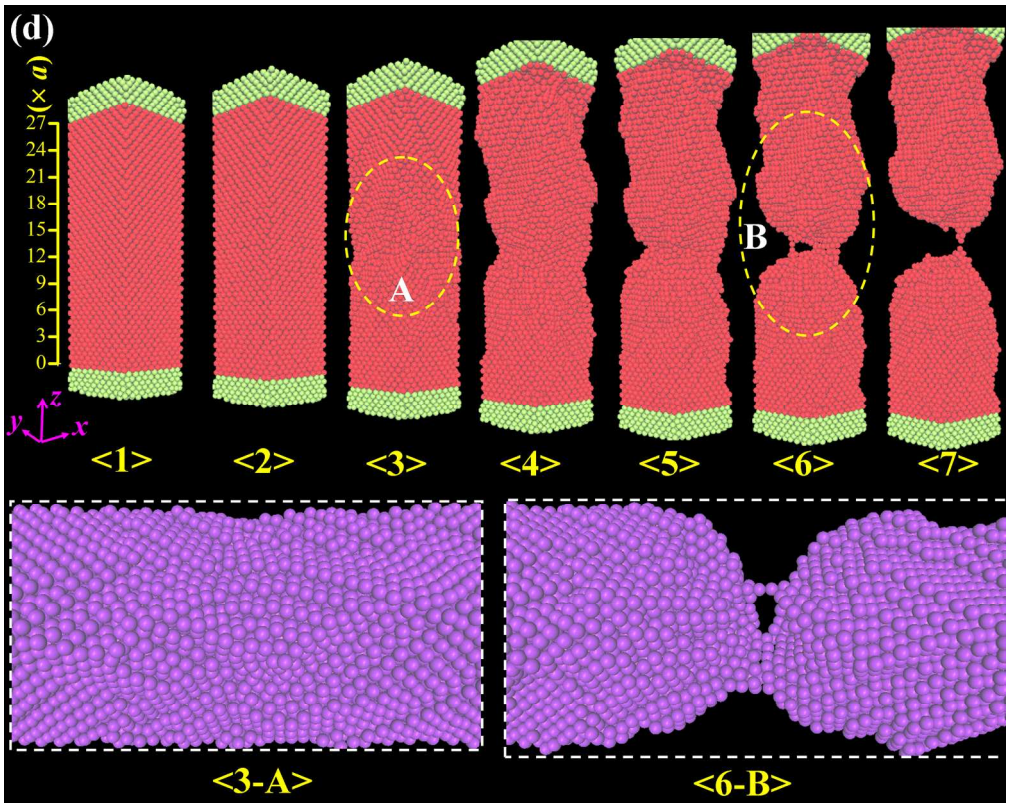

The deformation behavior of the nanowire under atomic vacancies.
99x79mm (600 x 600 DPI)

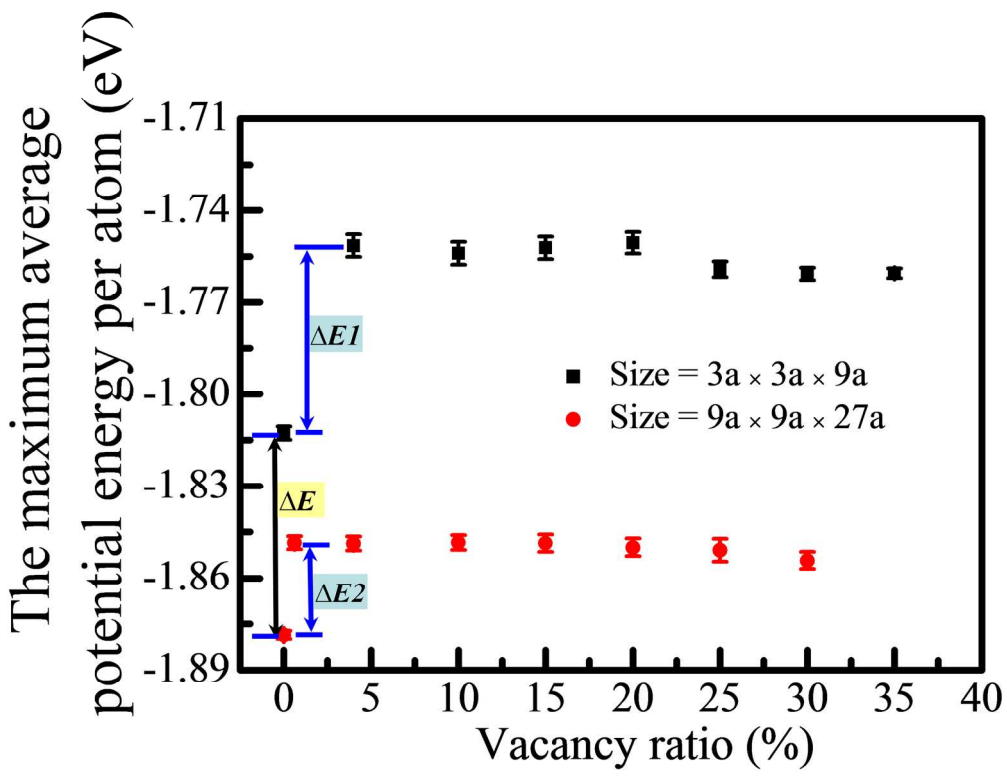

The maximum average potential energy per atom of the [100] single-crystal gold nanowire plotted against atomic vacancy ratio at two different sizes.
96x75mm (600 x 600 DPI)

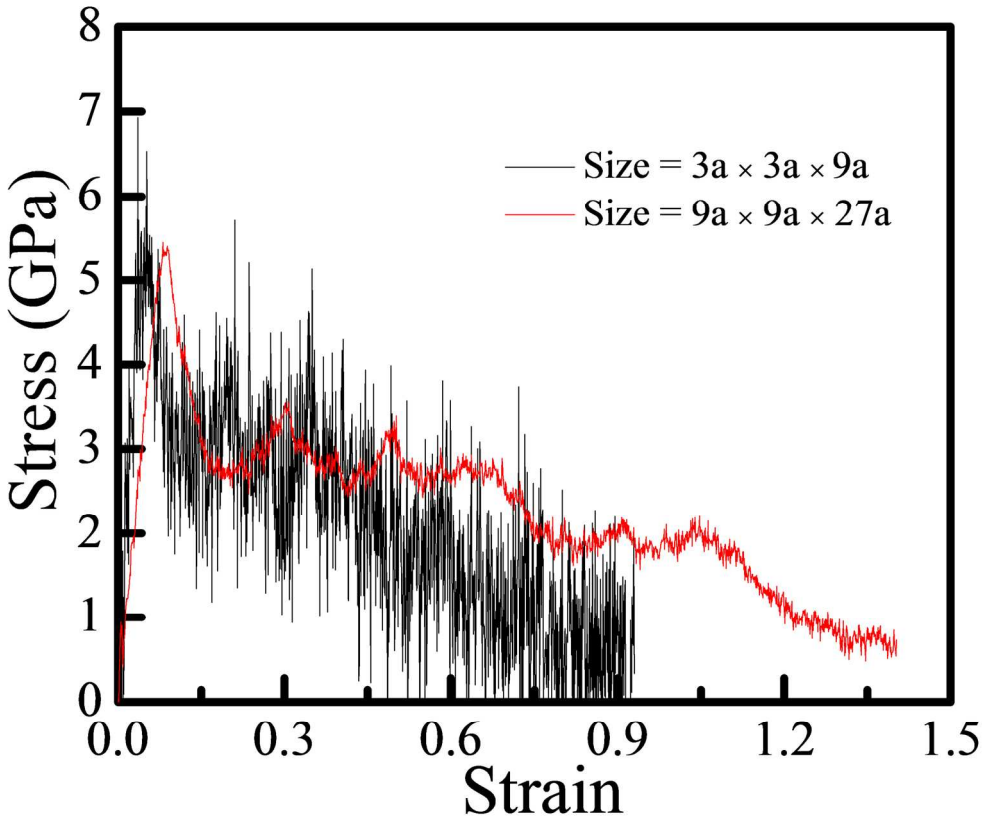

The representative stress-strain relationship of the nanowire at two different sizes
95x79mm (600 x 600 DPI)

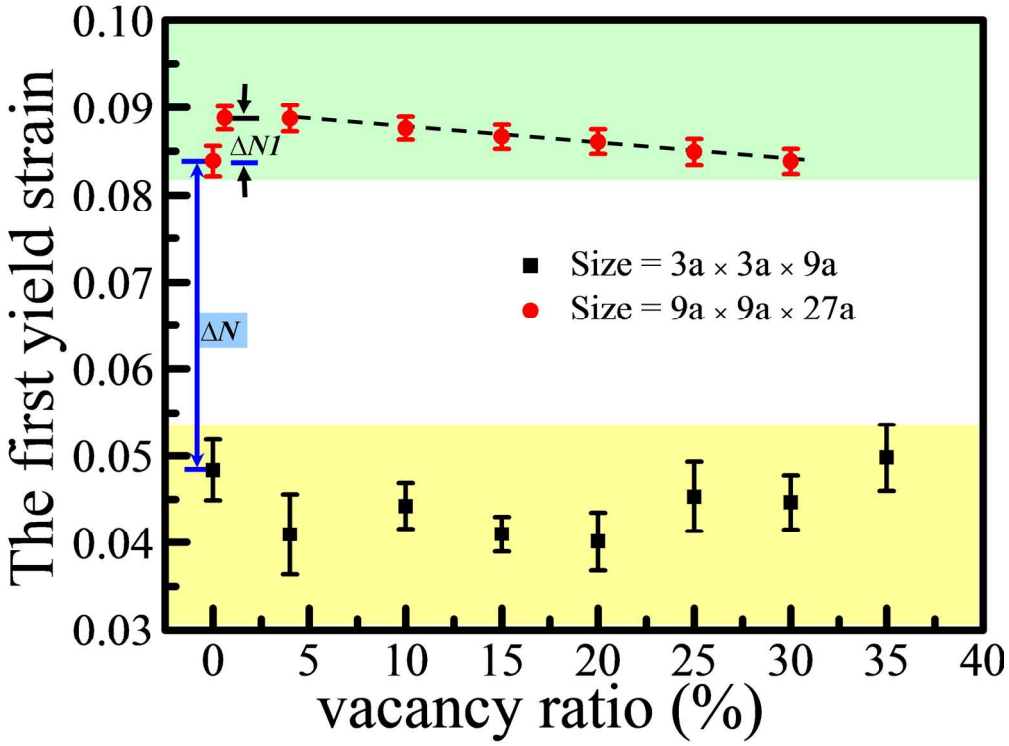

The first yield strain of the nanowire plotted against atomic vacancy ratio at two different sizes
93x70mm (600 x 600 DPI)

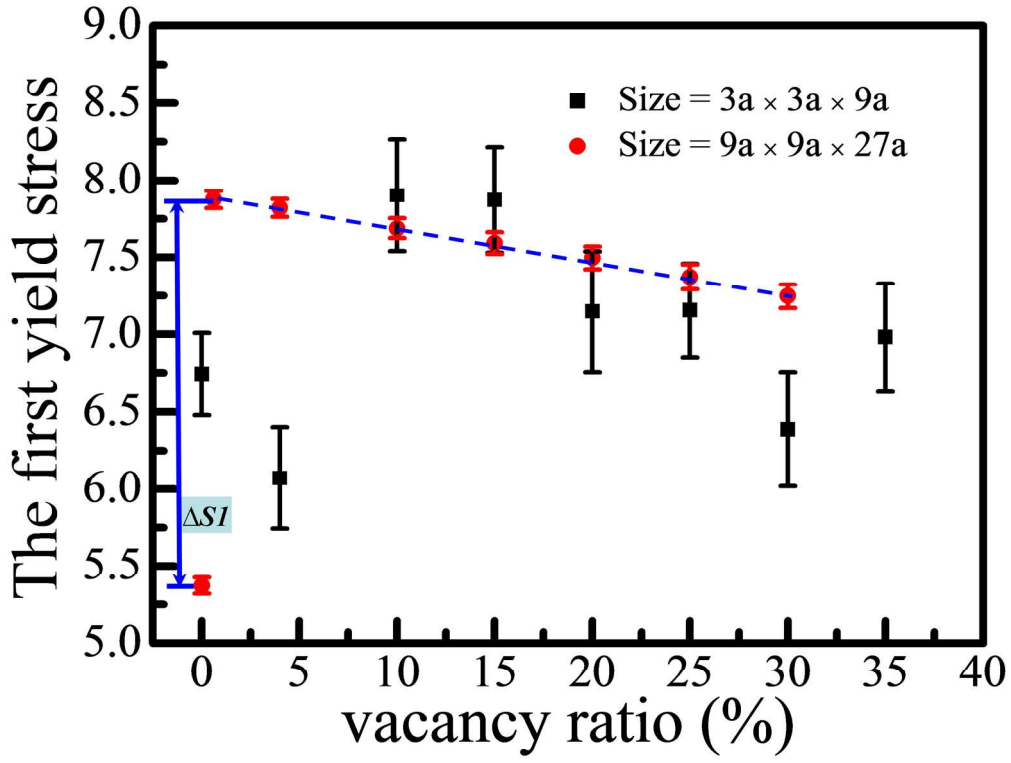

The first yield stress plotted against atomic vacancy ratio at two different sizes
96x73mm (600 x 600 DPI)

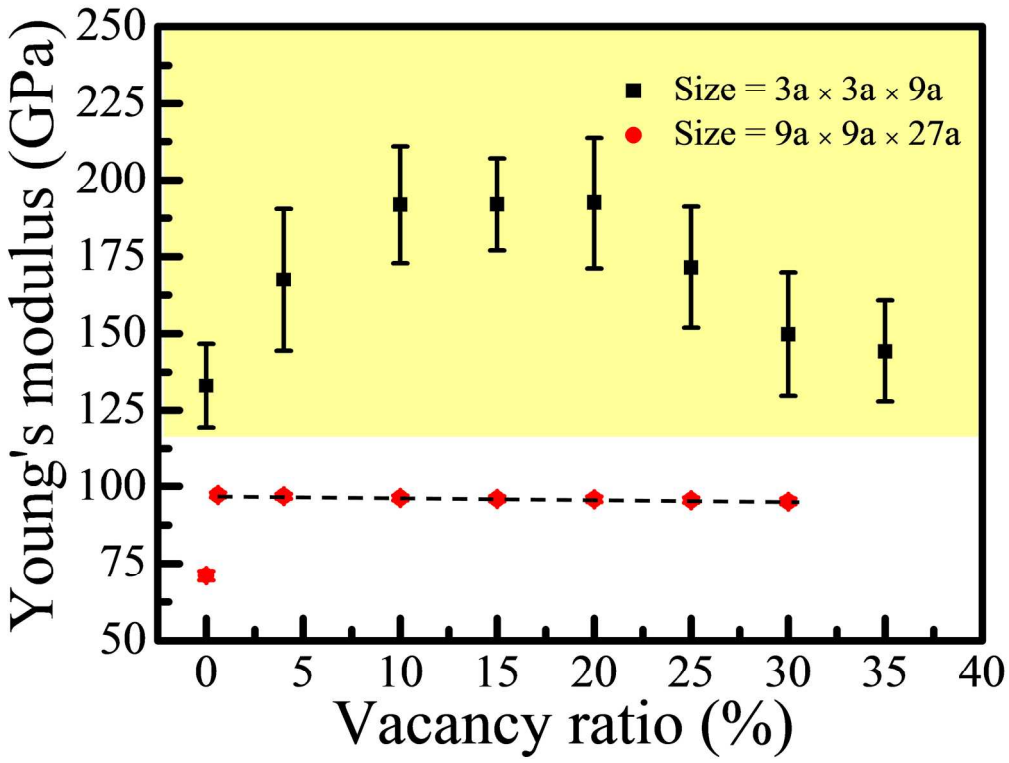

Young's modulus plotted against atomic vacancy ratio at two different sizes
96x74mm (600 x 600 DPI)